Coherence in charge and energy transfer in molecular junctions

Alexander J. White,[1,*] Uri Peskin,[2,†] and Michael Galperin[1,‡]
[1]*Department of Chemistry & Biochemistry, University of California San Diego, La Jolla, California 92093, USA*
[2]*Schulich Faculty of Chemistry and the Lise Meitner Center for Computational Quantum Chemistry, Technion-Israel Institute of Technology, Haifa 32000, Israel*
(Received 12 May 2013; revised manuscript received 15 July 2013; published 25 November 2013)

We consider the effects of dephasing on field-induced coherent charge and energy transport in molecular junctions. Within generic models we show that dephasing controls the relative intensities of energy and charge fluxes, and that the dependence of the energy flux on the dephasing rate is nonmonotonic. We further demonstrate the possibility for laser-controlled charge-energy separation in multiterminal molecular junctions, a prerequisite for engineering low-heating stable nanoscale devices.

DOI: 10.1103/PhysRevB.88.205424 PACS number(s): 85.65.+h, 73.22.Lp, 84.30.Jc, 85.35.Ds

I. INTRODUCTION

Single molecules are promising candidates for integration into nanoscale devices. Based on the versatility in structural, electronic, optical, and mechanical properties of molecules, molecular devices can be carefully designed and controlled. The small size of molecules implies the necessity of quantum mechanical treatment, and naturally poses questions on the role of coherences in the response properties of molecular devices. In molecular junctions experimental observations were attributed to interference effects in intramolecular electron transfer[1] and elastic transport through single molecules,[2,3] or to vibrationally induced decoherence.[4]

Coherent control in molecules originated in studies of quantum dynamics in response to laser pulse excitations.[5,6] Advances in optics combined with molecular fabrication techniques in junctions resulted in a new field termed molecular optoelectronics.[7,8] Coherent control of transport in molecular junctions is one of the focuses of research in this field.[9–14] Another focus is the dynamics of energy transfer between plasmonic and molecular excitations.[15–19] The importance of quantum coherence in energy transfer was demonstrated recently in studies of the initial stages of photosynthesis.[20–24]

Theoretical studies in molecular electronics are mostly focused on the role of coherence in elastic transport. In particular, a molecular switch based on quantum interference was proposed in Refs. 25 and 26, and molecular transistors utilizing coherence to control transport through single molecule junctions (usually containing a conjugated π system) were discussed in Refs. 27–33. Inelastic processes are usually considered as a source of decoherence, which can both destroy[34,35] or enhance[35–38] transport through molecular systems. Coherence induced by inelastic processes was observed experimentally[39] and discussed in several theoretical studies.[35,40,41] Finally, coherent and incoherent exciton transport in the Fenna-Matthews-Olson complex was studied in a number of theoretical publications.[42–46]

In molecular optoelectronics[8] it is customary to distinguish between charge and energy transfer processes between the molecule and contacts (as well as inside the molecular complex). For example, elastic electron transport (single charges moving through the system) is at the heart of charge transfer–surface enhanced Raman spectroscopy (CT-SERS),[47,48] while pure energy transfer (transfer of excitation without charge transfer) accounts for coupling between molecular excitations and excitations of the leads (excitonlike or neutral pairings of electronlike and holelike excitations).[17,49–53] Considering nonequilibrium transport through molecular junctions, charge and energy transport processes happen simultaneously, and a rigorous description must therefore account for this. The nonquadratic character of the energy transfer matrix elements complicates the theoretical description and the corresponding theoretical considerations usually rely on approximations.[54,55] Recently we proposed a pseudoparticle nonequilibrium Green's functions (PP-NEGF) method as a tool capable to treat the processes simultaneously and exactly.[52]

Contrary to previous studies where the effects of coherence in either charge or energy transfer were discussed, here we apply the PP-NEGF approach and consider the importance of coherences in simultaneous charge and energy transport through molecular junctions. In particular, we demonstrate possibilities for laser-induced coherent control of the relative magnitude of energy and charge fluxes generated by a molecular pump. Inspired by the known effect of charge and spin separation in molecular systems[56–59] we also demonstrate a possibility to coherently control the spatial separation of charge and energy fluxes in properly designed multiterminal molecular junctions.

The different response of charge and energy flows to an external field is derived from the different underlying laser-matter interactions. Energy transport is due to dipole coupling between molecular excitations to electron-hole or plasmon excitations in the leads (usually treated as dipole-dipole interactions), while charge transport is modeled as electron tunneling.[49] Therefore, matrix elements for energy and charge transport between given chromophores can differ in magnitude or phase. In simple cases the different matrix elements can be associated with different Rabi frequencies for charge and energy transfer through the molecule, and when one of these frequencies is in resonance with optically induced Rabi oscillations, the corresponding flux (energy or charge) is expected to be maximal. For realistic systems the task of optimizing the external field parameters for a selected process (amplitude and frequency) is more involved, but nevertheless, we still claim that conditions can be defined in which the field selectively enhances (or suppresses) charge flux along a given path and energy flux along another. As far as we know, this is

the first time when the possibility of such separation between charge and energy fluxes is discussed.

In the following we consider explicitly only energy transfer within the molecule. Heat transfer between the molecule and the leads is not accounted for, assuming a constant junction temperature. Note that both charge transport (emission of energetic electrons) and energy transport (emission of electron-hole pairs) can induce heating in the leads, however these processes are external to the molecule, and take place far from the junction.[60] Thus, their effect on the transport at the molecular junction can be neglected. As a side note we mention that the description of molecular excitation (energy transfer) we consider is technically similar to modeling the propagation of vibrational excitation (phonon transport) when expressed in the language of vibronic states. Thus our findings may have implications also in the context of low heating stable nanoscale devices.

Below, after introducing two generic models for charge/energy pump and switch, we discuss a convenient methodology for treating the combined intramolecular electron and energy transfer. Our numerical simulations demonstrate different possibilities for laser control of coherent molecular energy and charge pumps, and for spatial separation of charge and energy fluxes in molecular junctions.

II. MODEL

We consider a network of N_m molecules, characterized by chromophores which are coupled to several reservoirs of electrons (or contacts C) and thermal baths (B). The contacts are assumed to be in equilibrium (no bias), and the driving of the junctions is governed by a laser field $E(t)$ applied to one of the molecules. Each molecular chromophore is represented by its highest occupied (HOMO) and lowest unoccupied (LUMO) molecular orbitals (or ground g and excited x states). We consider electron and energy transfer between neighboring chromophores and between the chromophores and the baths. We emphasize that our models focus on energy transport through the molecule and does not account explicitly for the thermalization process of access energy in the leads, which happens far from the junction region.

Two systems are discussed: The first model corresponds to a molecular charge and energy pump [$N_m = 4$, see Fig. 1(a)], based on bridge-mediated (1 and 2) transfer between a donor (0) and an acceptor (3). The donor and acceptor are coupled to their own contacts and thermal baths, and the donor is driven by an external laser field. The bridge contains two molecules and the coherent transport reflects interference between the two possible pathways. In order to induce decoherence, one of the bridge molecules (1) is coupled to a local dephasing source (B_d). This type of model is frequently used in considerations of effects of decoherence on electron transfer.[34,36,40]

The second model [$N_m = 3$, see Fig. 1(b)] corresponds to a molecular switch with a donor (0) and two acceptors (1 and 2), each coupled to its own contact and thermal bath. As previously, the donor is driven by an external laser field. We used this model in our previous study[14] as a prototype of a coherently controlled molecular switch. Here we extend the consideration to the case of simultaneous energy and charge transfer.

The Hamiltonian of the system(s) is

$$\hat{H}(t) = \hat{H}_M(t) + \sum_K (\hat{H}_K + \hat{V}_{MK}), \tag{1}$$

where $\hat{H}_M(t)$ and $\hat{H}_K$ describe the molecular system M and bath K (K is summed over all the baths in the model), and $\hat{V}_{MK}$ is the coupling between the two. The explicit expressions are

$$\begin{aligned}\hat{H}_M(t) &= \sum_{m=0}^{N_m} \sum_{\ell=g,x} \varepsilon_{m\ell} \hat{n}_{m\ell} - \mu_0 E_0 (\hat{d}_{0x}^\dagger \hat{d}_{0g} e^{-i\omega_0 t} + \text{H.c.}) \\ &+ \sum_{m,m'=0}^{N_m} \left(\sum_{\ell=g,x} t_{m\ell,m'\ell} \hat{d}_{m\ell}^\dagger \hat{d}_{m'\ell} + J_{m,m'} \hat{D}_m^\dagger \hat{D}_{m'} + \text{H.c.} \right),\end{aligned} \tag{2}$$

$$\hat{H}_{C_m} = \sum_{\kappa \in C_m} \varepsilon_\kappa \hat{n}_\kappa, \quad \hat{H}_{B_m} = \sum_{\alpha \in B_m} \omega_\alpha \hat{n}_\alpha, \tag{3}$$

$$\begin{aligned}\hat{V}_{MC_m} &= \sum_{\kappa \in C_m} \sum_{\ell=g,x} (V_{\kappa,m\ell} \hat{c}_\kappa^\dagger \hat{d}_{m\ell} + \text{H.c.}), \\ \hat{V}_{MB_m} &= \sum_{\alpha \in B_m} (U_{\alpha,m} \hat{a}_\alpha^\dagger \hat{D}_m + \text{H.c.}).\end{aligned} \tag{4}$$

In the molecular pump model [Fig. 1(a)] local dephasing is introduced by coupling the LUMO of molecule 1 to the bath B_d,

$$\hat{H}_{B_d} = \sum_\beta \omega_\beta \hat{n}_\beta, \quad \hat{V}_{MB_d} = M \sum_\beta (\hat{b}_\beta + \hat{b}_\beta^\dagger) \hat{n}_{1x}. \tag{5}$$

In Eqs. (2)–(5) $\hat{d}_{m\ell}^\dagger$ and $\hat{c}_\kappa^\dagger$ create electrons in level ℓ of molecule m, and state κ of contacts $\{C_m\}$, respectively, and $\hat{a}_\alpha^\dagger$ and $\hat{b}_\beta^\dagger$ create phonons in the thermal baths $\{B_m\}$ and B_d, respectively. $\hat{n}_{m\ell} \equiv \hat{d}_{m\ell}^\dagger \hat{d}_{m\ell}$, $\hat{n}_\kappa \equiv \hat{c}_\kappa^\dagger \hat{c}_\kappa$, $\hat{n}_\alpha \equiv \hat{a}_\alpha^\dagger \hat{a}_\alpha$, and $\hat{n}_\beta \equiv \hat{b}_\beta^\dagger \hat{b}_\beta$ are population operators. $\hat{D}_m^\dagger \equiv \hat{d}_{mx}^\dagger \hat{d}_{mg}$ is the operator of molecular excitation. $\varepsilon_{m\ell}$ and ε_κ are on-site electronic energies of level $m\ell$ in the molecules and state k in the contacts. ω_α and ω_β are elementary excitations in the thermal baths $\{B_m\}$ and B_d, respectively. μ_0 is the transition dipole moment of the donor, and E_0 and ω_0 are the amplitude of the driving field and its frequency. $t_{m\ell,m'\ell}$ and $J_{m,m'}$ are the matrix elements of charge and energy transfer between the chromophores m and m', where the pathways are indicated by lines in Fig. 1. Finally, $V_{\kappa,m\ell}$ and $U_{\alpha,m}$ represent electron and energy exchange between the chromophores and the baths and M is the dephasing strength. We note that coupling to the driving field is written in the rotating wave approximation. Similar models for electron and energy (exciton) transport were considered in the literature previously.[49,54,55]

A transformation to the rotating frame of the field[14]

$$\hat{\tilde{H}} = i \left(\frac{\partial}{\partial t} e^{\hat{S}(t)} \right) e^{-\hat{S}(t)} + e^{\hat{S}(t)} \hat{H} e^{-\hat{S}(t)}, \tag{6}$$

where

$$\hat{S}(t) \equiv \frac{i\omega_0 t}{2} \sum_{m=1}^{N_m} \left(\hat{n}_{mx} - \hat{n}_{mg} + \sum_{\kappa \in C_m} \hat{n}_\kappa + \sum_{\alpha \in B_m} \hat{n}_\alpha \right) \tag{7}$$

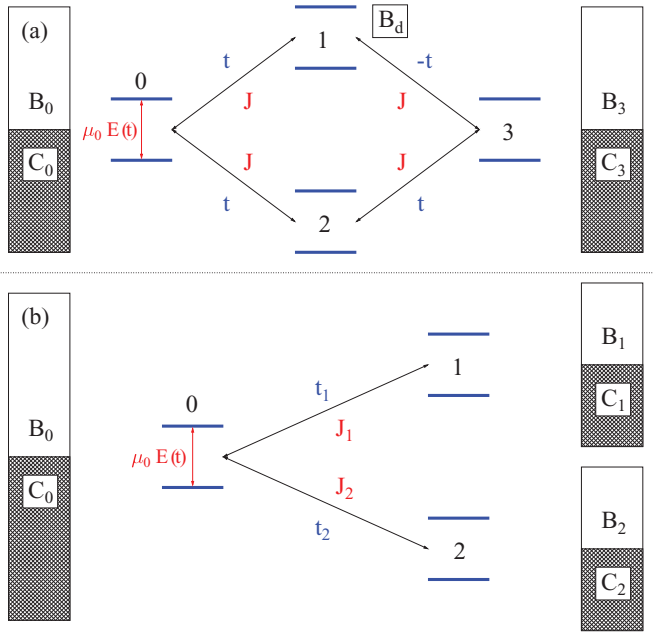

FIG. 1. (Color online) A sketch of the models for coherently controlled charge-energy (a) pump and (b) switch.

represents the model in terms of effective time-independent Hamiltonian $\hat{\tilde{H}}$, which is given by Eqs. (2)–(5) with $\varepsilon_{mg} \to \varepsilon_{mg} + \omega_0/2$, $\varepsilon_{mx} \to \varepsilon_{mx} - \omega_0/2$, and $\mu_0 E_0 \exp(\pm i\omega_0 t) \to \mu_0 E_0$. As a result of the transformation one also has to consider different positions of the electrochemical potentials in the contacts for the x (shifted by $\omega_0/2$ downward) and the g (shifted by $\omega_0/2$ upward) molecular orbitals (see Appendix A for details). Note that the time-independent formulation is possible only in the case of relatively weak molecule-baths couplings, when effective second order is sufficient and bath-induced cross correlations between ground and excited molecular levels can be disregarded.[56,61–63]

As discussed in our previous publication[52] the pseudoparticle nonequilibrium Green function (PP-NEGF) formalism is especially convenient for studies where combined electron and energy transfers play an important role. The PP-NEGF treats all the interactions in the molecule exactly, by representing the molecular part of the Hamiltonian in the basis of many-body states of an isolated molecule. Here we employ the PP-NEGF to the models (2)–(5). The pseudoparticles, introduced in an extended Hilbert space, correspond to the many-body states $\{|S\rangle\}$ of the molecular system. The physical subspace is defined by the constraint $\sum_S \hat{p}_S^\dagger \hat{p}_S = 1$, where $\hat{p}_S^\dagger$ ($\hat{p}_S$) is the operator of creation (annihilation) of the many-body state $|S\rangle$. In the extended Hilbert space the usual rules of quantum field theory are applicable. In particular, the pseudoparticle Green function (GF) on the Keldysh contour

$$G_{SS'}(\tau,\tau') \equiv -i\langle T_c\, \hat{p}_S(\tau)\, \hat{p}_{S'}(\tau')\rangle \tag{8}$$

satisfies the Dyson equation. A self-consistent procedure for numerical evaluation of the projections of the GF can be formulated in the physical subspace (see, e.g., Ref. 64 for details). After the procedure converges, the resulting projections of the GF can be used to calculate charge I_m^c and energy I_m^E currents at the interface between the molecular system and the baths C_m and B_m, respectively. Below we perform analysis within the noncrossing approximation (see, e.g., Ref. 64 for details). The approximation works well for weak molecule-baths coupling, when the parameters describing coupling to the baths are small relative to all other relevant energy scales in the system. In our case the latter are the HOMO-LUMO gap and intramolecular hopping parameters. Weak coupling to baths makes the processes of molecule-bath interactions rare, thus justifying a noncrossing approximation, i.e., treating the processes sequentially. At steady state, this leads to the following explicit expressions for the fluxes (see Appendix B for the derivation):[52,64]

$$I_m^c = -\frac{e}{\pi h} \sum_{\substack{S_1,S_2\\S_3,S_4}} \mathrm{Re} \int_{-\infty}^{+\infty} dE \int_{-\infty}^{+\infty} d\epsilon\, \zeta_2\, G_{24}^<(E) \times\left[\Sigma_{12,34}^{C_m,<}(\epsilon) G_{31}^r(E+\epsilon) + \Sigma_{43,21}^{C_m,>}(\epsilon) G_{31}^r(E-\epsilon)\right], \tag{9}$$

$$I_m^E = \frac{1}{\pi h} \sum_{\substack{S_1,S_2\\S_3,S_4}} \mathrm{Re} \int_{-\infty}^{+\infty} dE \int_{0}^{\infty} d\omega\, \omega\, \zeta_2\, G_{24}^<(E) \times\left[\Pi_{12,34}^{B_m,<}(\omega) G_{31}^r(E+\omega) + \Pi_{43,21}^{B_m,>}(\omega) G_{31}^r(E-\omega)\right], \tag{10}$$

where $G_{pq}^{r(<)}(E) \equiv G_{S_p S_q}^{r(<)}(E)$ is the Fourier transform of the retarded (lesser) projection of the GF (8), $\zeta_p = 1$ (-1) for the bosonic (fermonic) state $|S_p\rangle$,[64] and $\Sigma^{C_m,\gtrless}$ ($\Pi^{B_m,\gtrless}$) are greater/lesser projections of the molecular system self-energy due to coupling to bath C_m (B_m),

$$\Sigma_{12,34}^{C_m,\gtrless}(\epsilon) \equiv \mp i \sum_{m\ell,m'\ell'} \xi_{12}^{m\ell} \Gamma_\ell^{C_m} \xi_{34}^{*m'\ell'} F_{C_m}^{\gtrless}(\epsilon), \tag{11}$$

$$\Pi_{12,34}^{B_m,\gtrless}(\omega) \equiv -i \sum_{m,m'} \chi_{12}^{m} \Omega^{B_m} \chi_{34}^{*m'} F_{B_m}^{\gtrless}(\omega). \tag{12}$$

Here $F_{C_m}^>(\epsilon) \equiv 1 - f_{C_m}(\epsilon)$, $F_{C_m}^<(\epsilon) \equiv f_{C_m}(\epsilon)$, $F_{B_m}^>(\omega) \equiv 1 + N_{B_m}(\omega)$, $F_{B_m}^<(\omega) \equiv N_{B_m}(\omega)$; $f_{C_m}(\epsilon)$ and $N_{B_m}(\omega)$ are Fermi-Dirac and Bose-Einstein distributions,

$$\Gamma_\ell^{C_m} \equiv 2\pi \sum_{\kappa\in C_m} |V_{\kappa,m\ell}|^2 \delta(\epsilon - \epsilon_\kappa), \tag{13}$$

$$\Omega^{B_m} \equiv 2\pi \sum_{\alpha\in B_m} |U_{\alpha,m}|^2 \delta(\omega - \omega_\alpha) \tag{14}$$

are dissipation rates due to coupling to baths C_m and B_m, $\xi_{pq}^{m\ell} \equiv \langle S_p|\hat{d}_{m\ell}^\dagger|S_q\rangle$, and $\chi_{pq}^m \equiv \langle S_p|\hat{D}_m^\dagger|S_q\rangle$.

III. NUMERICAL RESULTS

Here we consider charge (9) and energy (10) fluxes in the molecular pump and switch models [Figs. 1(a) and 1(b)], Eqs. (2)–(5). Unless stated otherwise the calculations are performed for the following "standard" set of parameters: $T = 300$ K, $\varepsilon_{0g} = -1$ eV, $\varepsilon_{0x} = 1$ eV, $\omega_0 = 2$ eV, $t_{mg,m'g} = 0$, $t_{mx,m'x} = J_{m,m'} = 10$ meV, $\Gamma_\ell^{C_m} = \Omega^{B_m} = 2.5$ meV ($m,m' \in \{1,\ldots,N_m\}$). The Fermi energy is taken at the origin $E_F = 0$ and the calculations are performed on an adaptive energy grid.

We note that these model parameters are chosen to be in a physically relevant range. In particular, the molecular HOMO-LUMO gaps $\varepsilon_{mx} - \varepsilon_{mg}$ are assigned typical values of 2 eV, which is accessible by lasers in the near infrared part of the spectrum. The escape rates Γ^{C_m} are chosen in accordance with experimental data on lifetime for the decay of an excess electron on a molecule near a metal surface.[65] These parameters lead to charge fluxes on the order of nA and heat fluxes on the order of nW, both are well within the measurable region (see, e.g., Refs. 66 and 67 for measurable charge and heat flux estimates, respectively).

A. Molecular pump

First we consider the charge-energy pump model. In the absence of dephasing at the bridge the transport of both charge and energy through the molecule is coherent, and depends on interference between two independent paths from the donor (0) to the acceptor (3) through molecules 1 and 2 [see Fig. 1(a)]. For the case of identical (degenerate) chromophores as considered here, the interference is controlled by the relative magnitudes and phases of the coupling matrix elements (the "J"s and the "t"s) along the different paths. In the particular design considered in Fig. 1(a), destructive interference does not allow charge flux through the system, whereas energy flux is favored in this case due to constructive interference. The spatial separation between the two bridge chromophores allows one to selectively control the transport by coupling one of the chromophores to a local source of dephasing. The latter is introduced by coupling the LUMO of one of the bridge chromophores (1) to a bath [B_d, Eq. (5)] of harmonic oscillators, assumed to be in their ground state. To restrict the effect of this perturbation to pure dephasing, a limit of $\omega_\beta \to 0$ is taken (such that energy exchange with this particular bath is excluded). This results in a self-energy (see Appendix C for details)

$$\Sigma^{B_d,\gtrless}_{12,34} \equiv -i\eta^{1x}_{12}\,\gamma^{B_d}\,\eta^{*1x}_{34}, \tag{15}$$

where $\gamma^{B_d} \equiv 2\pi M^2 \rho_{B_d}$ is *the dephasing rate*, ρ_{B_d} is density of modes in the bath B_d, and $\eta^{1x}_{pq} \equiv \langle S_p|\hat{n}_{1x}|S_q\rangle$. Note that the resulting expression is similar to the Buttiker probe model, which is widely used for introducing dephasing.

Figure 2 demonstrates the effect of increasing the dephasing rate on the two fluxes. As expected, the electric current (solid line) increases when destructive interference is suppressed. The energy flux (dashed line) shows a nonmonotonic behavior. An initial decrease in the flux with increasing dephasing rate, related to the suppression of constructive interference, is followed by an unexpected increase at higher dephasing rates. We attribute this behavior to competition between energy and charge transfer processes at molecule 1 for the same electronic population of its LUMO. Indeed, for weak dephasing, the charge delocalization among the LUMOs of chromophores 0, 1, and 3, is expected to hinder energy transfer between those molecules. Transition from coherent to hopping mechanism of charge transfer takes place at rates of dephasing $\gamma^{B_d} \sim t_{1x,0x}$ ($t_{1x,3x}$), leading to localization of electronic population at the bridge site $1x$ and (as a result) to an increase in energy flux.

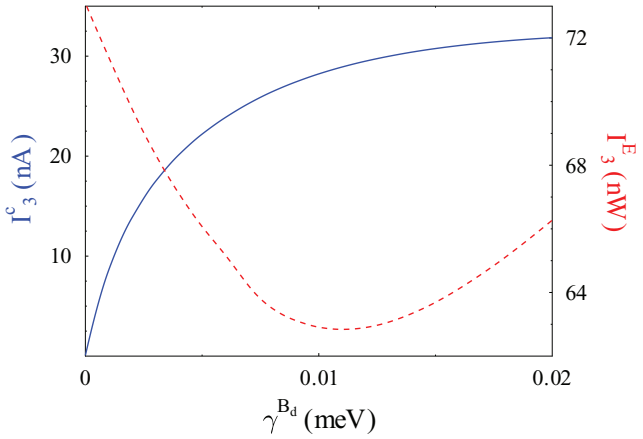

FIG. 2. (Color online) Molecular pump [Fig. 1(a)]. Shown are the charge [I^c_3, Eq. (9)—solid line, blue] and energy [I^E_3, Eq. (10)—dashed line, red] fluxes on the right interface as functions of dephasing rate γ^{B_d} [Eq. (15)]. See text for parameters.

It is interesting to note that controlling the dephasing can tune the molecular device between energy and charge pumping regimes.

B. Molecular switch

Having introduced the possibility of control over charge and energy fluxes, which are present simultaneously, we turn to examine the possibility of charge-energy separation in coherent transport through molecular devices. Note that effects of quantum coherence were observed experimentally (separately) for charge and energy (exciton) transport in molecular junctions. In some cases, such as in CT-SERS, charge and energy transfer are mixed coherently to define the overall optical response of a junction. Our consideration below suggests another possibility of observing coherence induced effects in charge and energy (exciton) transport in molecular junctions.

We consider a model of a molecular switch (1 b), where a single donor, driven by an external field, is coupled to two different acceptors. The versatility of molecular chromophores allows the design of different acceptors with different orbital energies and different coupling matrix elements to the donor. Therefore, coherent transport from the donor to each acceptor would be associated with characteristic Rabi frequencies, defined by the t and J hopping parameters for exchanging charge and energy with the donor. Our aim is to define conditions in which charge and energy fluxes are directed to different acceptors.

Figure 3(a) demonstrates a possibility of charge-energy separation in a molecular switch. The calculation is performed for $T = 10$ K, $\varepsilon_{1g} = -1.25$ eV, $\varepsilon_{1x} = 1.05$ eV, $\varepsilon_{2g} = -0.95$ eV, $\varepsilon_{2x} = 1.15$ eV, and $\Omega^{B_m} = 10$ meV. For these parameters at $\mu_0 E_0 \sim 50$ meV charge flux is directed to acceptor 1 (solid line), while energy flux to acceptor 2 (dash-dotted line). By tuning the amplitude of the laser field so that $\mu_0 E_0 \sim 150$ meV the direction of the fluxes is switched. Figure 3(b) demonstrates the possibility of control by the driving field frequency. Here $\varepsilon_{1g} = -1.1$ eV, $\varepsilon_{1x} = 1.05$ eV, $\varepsilon_{2g} = -0.9$ eV, $\varepsilon_{2x} = 1.15$ eV, and $\mu_0 E_0 = 10$ meV. As one can see, also in this case charge

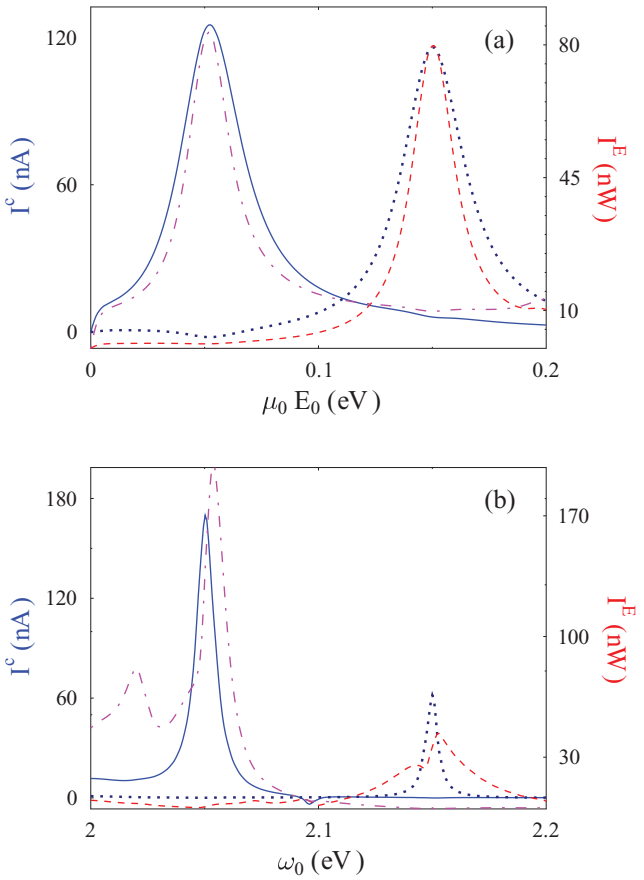

FIG. 3. (Color online) Molecular switch [Fig. 1(b)]. Shown are charge [I_1^c—solid line, blue; I_2^c—dotted line, dark blue; Eq. (9)], and energy [I_1^E—dashed line, red; I_2^E—dash-dotted line, magenta; Eq. (10)] fluxes as functions of (a) the driving amplitude $\mu_0 E_0$ and (b) frequency ω_0 [Eq. (2)]. See text for parameters.

and energy fluxes are picked at different field frequencies which facilitates their separation.

Notice that the results of Fig. 3, obtained by the PP-NEGF scheme, can be regarded as a numerically exact solution of the simultaneous charge/energy transport problem. Indeed, the present calculation accounts exactly for the many-body problem within the molecular space, and given the (realistically) small molecule-contacts coupling parameters considered here, the noncrossing approximation yields the correct result for the effects of the molecule-leads interaction Note that simpler methodologies, such as Redfield-based quantum master equation techniques in principle, can also account exactly for the many-body problem within the molecular space, but may be inapplicable at the physically relevant low temperature regime ($k_B T \leqslant \Gamma$),[68–70] or when degenerate many-body eigenstates are present in the system.[71]

In order to gain a qualitative understanding of the physics behind the observed charge-energy separation, simpler methodologies may be useful. We refer to a reduced model of a molecular dimer, represented as two TLS connected by electron t and exciton J hopping matrix elements. One TLS represents the donor chromophore of the molecular switch and the other represents an acceptor, corresponding, e.g., to the lower pathway of Fig. 1(b). The Fock space of this dimer is spanned by many-body states accounting for all possible populations of the four single particle levels. Within the scattering approach, the total fluxes are obtained as integrals over energy-dependent transmission probabilities with weighting factors defined by populations in the baths. The scattering amplitudes for charge and energy (exciton) transport across the dimer are defined by sequences of electron transfer steps, as, e.g., the ones shown in Fig. 4(a) [relevant many-body states in the two-electron charging block of the system are enumerated in Fig. 4(b)], and the corresponding transfer probabilities at energy E are therefore proportional to $T^c(E) = |G^r_{16}(E)|^2$ for charge transfer and $T^E(E) = |G^r_{13}(E)|^2$ for energy transfer, respectively. Here $G^r_{S_1 S_2}(E)$ is the matrix element of the retarded Green function. For simplicity we take the resolvent as a rough estimate of the corresponding retarded Green function $\mathbf{G}^r(E) = [E - \tilde{\mathbf{H}}^{(2)}_M + i\eta]^{-1}$, with η taken as 1 meV. The dependence of the transfer probabilities on the energy and on the model parameters is therefore defined by the spectrum of the many-body dimer Hamiltonian which defines the resolvent poles. Representation of the dimer Hamiltonian in the basis defined in Fig. 4(a) reads

$$\tilde{\mathbf{H}}^{(2)}_M = \begin{bmatrix} \varepsilon_{0g}+\varepsilon_{2g}+\omega_0 & -\mu_0 E_0 & 0 & 0 & 0 & 0 \\ -\mu_0 E_0 & \varepsilon_{0x}+\varepsilon_{2g} & -J & 0 & 0 & t \\ 0 & -J & \varepsilon_{0g}+\varepsilon_{2x} & \mu_0 E_0 & t & 0 \\ 0 & 0 & \mu_0 E_0 & \varepsilon_{0x}+\varepsilon_{2x}-\omega_0 & 0 & 0 \\ 0 & 0 & t & 0 & \varepsilon_{0g}+\varepsilon_{0x} & 0 \\ 0 & t & 0 & 0 & 0 & \varepsilon_{2g}+\varepsilon_{2x} \end{bmatrix}. \quad (16)$$

Maps of the charge T^c and energy (exciton) T^E transmission coefficients as functions of the energy E and the external driving field parameters are shown in Fig. 4(c) for the driving field amplitude $\mu_0 E_0$, and Fig. 4(d) for the field frequency ω_0. The other parameters of the calculation are the same as in Fig. 3.

Two points are noteworthy: (1) T^c and T^E have their maxima at different values of the external driving parameters, which is the basis for the charge-energy separation discussed above. (2) The energy transmission coefficient T^E has two maxima as a function of the driving field frequency ω_0 [see right panel in Fig. 4(d)], which is the reason for a multiple-peak structure of the energy flux presented in Fig. 3(b). We reemphasize that such qualitative considerations are helpful, and are brought here as an interpretation to, but not instead of, the numerically exact results. Similarly, formulating conditions for maximal fluxes, based on resonances between

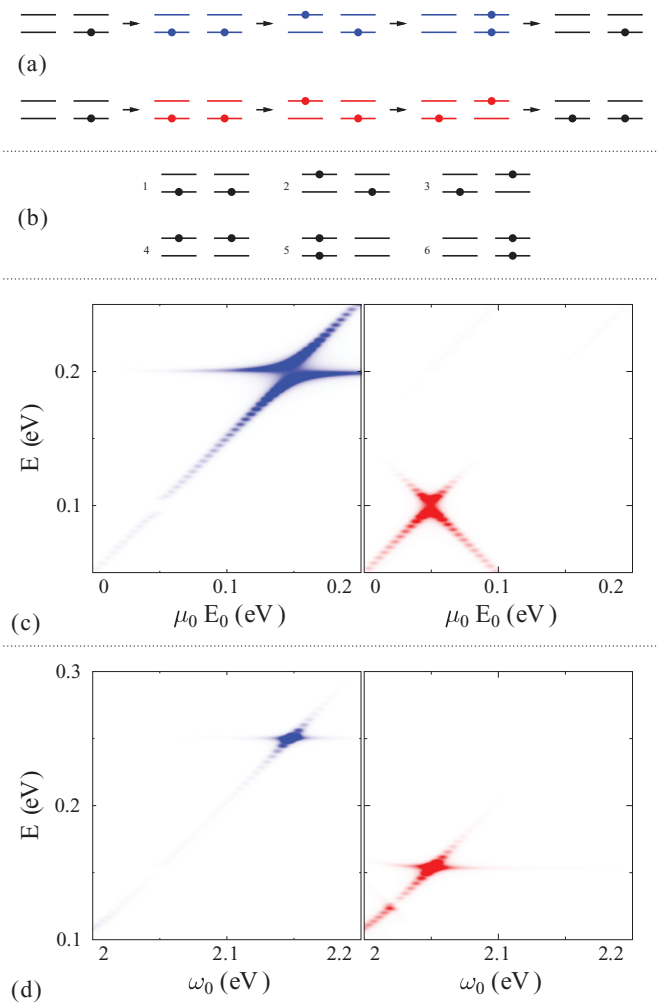

FIG. 4. (Color online) Molecular dimer. Shown are (a) schemes for charge (top) and energy (bottom) transfer; (b) relevant many-body states of the molecule, charge $T^c(E)$ (left, blue) and energy $T^E(E)$ (right, red) transmission coefficients as functions of energy E; (c) the driving amplitude $\mu_0 E_0$; and (d) frequency ω_0. See text for details.

Rabi frequencies in the field-free system and Rabi frequency induced by the field (as was discussed in Ref. 14 for charge transport), can support the numerical analysis, but provides only qualitative estimates.

IV. CONCLUSION

We studied the effects of coherence on electron and energy fluxes in molecular junctions. First we discussed the effect of dephasing on coherent transport in a bridge model with two interfering pathways [see Fig. 1(a)]. The molecular bridge was designed to minimize charge flux through the system due to destructive interference, and to maximize energy flux due to constructive interference between the different paths. Inducing dephasing destroys coherence in the system which leads to the appearance of charge flux and decrease in energy transfer. Further increase of the dephasing rate (to the order of intermolecular electronic hopping parameter) unexpectedly results in an increase of the energy transfer. We argued that the effect is due to competition between charge and energy transport on the same electronic population in the LUMO of the bridge molecule. At strong dephasing, where the electron transport mechanism changes from coherent to hopping, charge localization at the molecular LUMO increases the efficiency of sequential energy transfer through the junction.

After demonstrating a possibility of coherent control over the two fluxes, we discussed the possibility of charge-energy separation in a molecular switch [see Fig. 1(b)]. In particular, we showed that by tuning the laser field parameters, the fluxes can be directed to different acceptors. Moreover, the directions of energy and charge fluxes can be reversed by adjusting the field amplitude and/or frequency.

The two different models demonstrate the controllability of charge and energy transport in junctions, in which coherences play a crucial role. The theoretical demonstration of charge-energy separation in a junction is a first step in the direction of engineering low-heating stable molecular nanoscale devices.

ACKNOWLEDGMENTS

We gratefully acknowledge support by the Department of Energy (M.G., Early Career Award, DE-SC0006422), the German-Israeli Science Foundation (U.P.), and the US-Israel Binational Science Foundation (U.P. and M.G., Grant No. 2008282).

APPENDIX A: TRANSFORMATION TO THE ROTATING FRAME OF THE FIELD

Here we discuss the transformation to the rotating frame of the field [Eq. (6)] and the formulation of the effective time-independent model. Applying the transformation to the rotating frame

$$\hat{A} \to e^{\hat{S}(t)} \hat{A} e^{-\hat{S}(t)}, \tag{A1}$$

with $\hat{S}(t)$ defined in Eq. (7), to the quasiparticle excitation operators yields

$$\begin{aligned} &\hat{d}_{mg} \to \hat{d}_{mg} e^{-i\omega_0 t/2}, \quad \hat{d}_{mx} \to \hat{d}_{mx} e^{i\omega_0 t/2}, \\ &\hat{c}_\kappa \to \hat{c}_\kappa e^{i\omega_0 t/2}, \quad \hat{a}_\alpha \to \hat{a}_\alpha e^{-i\omega_0 t/2}. \end{aligned} \tag{A2}$$

Together with additional terms due to the time-dependent correction [first term on the right side of Eq. (6)]

$$\frac{\omega_0}{2} \sum_{m=1}^{N_m} \left[\hat{n}_{mg} - \hat{n}_{mx} - \sum_{\kappa \in C_m} \hat{n}_\kappa - \sum_{\alpha \in B_m} \hat{n}_\alpha \right] \tag{A3}$$

this leads to the effective Hamiltonian of the form [compare with Eqs. (2)–(4)]

$$\begin{aligned} \hat{\tilde{H}}_M = &\sum_{m=0}^{N_m} \sum_{\ell=g,x} \bar{\varepsilon}_{m\ell} \hat{n}_{m\ell} - \mu_0 E_0 (\hat{d}_{0x}^\dagger \hat{d}_{0g} + \text{H.c.}) \\ &+ \sum_{m,m'=0}^{N_m} \left(\sum_{\ell=g,x} t_{m\ell,m'\ell} \hat{d}_{m\ell}^\dagger \hat{d}_{m'\ell} + J_{m,m'} \hat{D}_m^\dagger \hat{D}_{m'} + \text{H.c.} \right), \end{aligned} \tag{A4}$$

$$\hat{\tilde{H}}_{C_m} = \sum_{\kappa \in C_m} \left(\varepsilon_\kappa - \frac{\omega_0}{2} \right) \hat{n}_\kappa, \quad \hat{\tilde{H}}_{B_m} = \sum_{\alpha \in B_m} \left(\omega_\alpha - \frac{\omega_0}{2} \right) \hat{n}_\alpha, \tag{A5}$$

$$\hat{\tilde{V}}_{MC_m} = \sum_{\kappa\in C_m} (V_{\kappa,mg}\hat{c}^\dagger_\kappa \hat{d}_{mg} e^{-i\omega_0 t} + \hat{c}^\dagger_\kappa \hat{d}_{mx} + \text{H.c.}),$$
$$\hat{\tilde{V}}_{MB_m} = \sum_{\alpha\in B_m} (U_{\alpha,m}\hat{a}^\dagger_\alpha \hat{D}_m e^{i\omega_0 t/2} + \text{H.c.}), \tag{A6}$$

where $\bar{\varepsilon}_{mg} \equiv \varepsilon_{mg} + \omega_0/2$ and $\bar{\varepsilon}_{mx} \equiv \varepsilon_{mx} - \omega_0/2$.

Since coupling to the baths is treated within the effective second order, i.e., the irreducible self-energy is proportional to the second order in molecule-bath coupling, the time-dependent terms in the couplings [Eqs. (A6)] will (partially) compensate for the shift of excitation energies in the bath [Eqs. (A5)]. In particular, the compensation will yield an unaltered expression for the self-energies due to the coupling to the bosonic baths B_m. Expressions for the self-energies due to the coupling to the fermonic baths C_m will have the state energies of the baths shifted by $\omega_0/2$ upward (downward) for the g (x) level of the molecule. If the HOMO-LUMO gap $\varepsilon_{mx} - \varepsilon_{mg}$ is big relative to the electron escape rate Γ (a common scenario in molecular junctions, where $\varepsilon_{mx} - \varepsilon_{mg} \sim 2$ eV and $\Gamma \sim 0.1$ eV), one can describe the molecule-contacts coupling at an interface C_m as coupling to two independent baths: one with the chemical potential $\mu_{C_m} + \omega_0/2$ representing coupling of the HOMO, the other with the chemical potential $\mu_{C_m} - \omega_0/2$ representing coupling of the LUMO. Such consideration results in an effective time-independent Hamiltonian for the originally time-dependent problem.

APPENDIX B: CHARGE AND ENERGY FLUXES IN THE NCA WITHIN PP-NEGF

Here we discuss the derivation of Eqs. (9) and (10). The starting points are expressions for charge and energy (phonon-assisted) fluxes within the nonequilibrium Green functions (NEGF) technique. At steady state the fluxes at the interface between molecule and baths C_m or B_m, respectively, are[72,73]

$$I^c_m = \frac{e}{\hbar}\int_{-\infty}^{+\infty}\frac{d\varepsilon}{2\pi}\sum_{m\ell,m'\ell'} \times\left[\Sigma^{C_m,<}_{m\ell,m'\ell'}(\varepsilon)\, G^{>}_{m'\ell',m\ell}(\varepsilon) - \Sigma^{C_m,>}_{m\ell,m'\ell'}(\varepsilon)\, G^{<}_{m'\ell',m\ell}(\varepsilon)\right], \tag{B1}$$

$$I^E_m = -\frac{1}{\hbar}\int_0^{\infty}\frac{d\omega}{2\pi}\omega\sum_{m,m'} \times\left[\Pi^{B_m,<}_{m,m'}(\omega)\, D^{>}_{m',m}(\omega) - \Pi^{B_m,>}_{m,m'}(\omega)\, D^{<}_{m',m}(\omega)\right], \tag{B2}$$

where $G^{\gtrless}$ and $D^{\gtrless}$ are the greater/lesser projections of the fermion and boson Green functions, respectively, defined on the Keldysh contour as

$$G_{m\ell,m'\ell'}(\tau,\tau') \equiv -i\langle T_c\, \hat{d}_{m\ell}(\tau)\, \hat{d}^\dagger_{m'\ell'}(\tau')\rangle, \tag{B3}$$

$$D_{m,m'}(\tau,\tau') \equiv -i\langle T_c\, \hat{D}_m(\tau)\, \hat{D}^\dagger_{m'}(\tau')\rangle. \tag{B4}$$

Here τ and τ' are the contour variables, T_c is the contour ordering operator, and operators $\hat{d}_{m\ell}$ and $\hat{D}_m$ are introduced below Eq. (5). Σ^{C_m} and Π^{B_m} are self-energies due to the coupling to fermonic bath C_m and bosonic bath B_m, respectively. Explicit expressions are[72,73]

$$\Sigma^{C_m,<}_{m\ell,m'\ell'}(\varepsilon) = i\,\Gamma^{C_m}_{m\ell,m'\ell'}(\varepsilon)\, f_{C_m}(\varepsilon), \tag{B5}$$

$$\Sigma^{C_m,>}_{m\ell,m'\ell'}(\varepsilon) = -i\,\Gamma_{m\ell,m'\ell'}(\varepsilon)[1 - f_{C_m}(\varepsilon)], \tag{B6}$$

$$\Pi^{B_m,<}_{m,m'}(\omega) = -i\,\Omega^{B_m}_{m,m'}(\omega)\, N_{B_m}(\omega), \tag{B7}$$

$$\Pi^{B_m,>}_{m,m'}(\omega) = -i\,\Omega^{B_m}_{m,m'}(\omega)[1 + N_{B_m}(\omega)]. \tag{B8}$$

Here $f_{C_m}(\varepsilon)$ and $N_{B_m}(\omega)$ are the Fermi-Dirac and Bose-Einstein thermal distributions in the baths C_m and B_m, respectively, and

$$\Gamma^{C_m}_{m\ell,m'\ell'}(\varepsilon) \equiv \sum_{\kappa\in C_m} V_{m\ell,\kappa}\, V_{\kappa,m'\ell'}\,\delta(\varepsilon - \varepsilon_\kappa), \tag{B9}$$

$$\Omega^{B_m}_{m,m'}(\omega) \equiv \sum_{\alpha\in B_m} U_{m,\alpha}\, U_{\alpha,m'}\,\delta(\omega - \omega_\alpha) \tag{B10}$$

are the dephasing matrices due to coupling to the baths. Note that in the paper we assume the wide-band approximation for both matrices[74,75] [see Eqs. (13) and (14)].

Spectral decomposition of the quasiparticle Fermi $\hat{d}^\dagger_{m\ell}$ and Bose $\hat{D}^\dagger_m$ excitation operators yields the connection to the pseudoparticle creation and annihilation operators $\hat{p}^\dagger_S$ and $\hat{p}_S$,

$$\hat{d}^\dagger_{m\ell} = \sum_{S_1,S_2} \xi^{m\ell}_{12}\, \hat{p}^\dagger_{S_1}\hat{p}_{S_2}, \tag{B11}$$

$$\hat{D}^\dagger_m = \sum_{S_1,S_2} \chi^{m}_{12}\, \hat{p}^\dagger_{S_1}\hat{p}_{S_2}, \tag{B12}$$

where $\xi^{m\ell}_{pq}$ and χ^{m}_{pq} are introduced below Eqs. (13) and (14), and $|S_1\rangle$ and $|S_2\rangle$ are molecular many-body states. Substituting Eqs. (B11) and (B12) into the lesser and greater projections of the definitions of the Green functions Eqs. (B3) and (B4), and using properties of the noncrossing approximation,[76] leads to the connection between the quasi- and pseudoparticles Green functions

$$G^{<}_{m\ell,m'\ell'}(t,t') = -i\sum_{\substack{S_1,S_2\\S_3,S_4}} \zeta_2\, \overset{*}{\xi}{}^{m\ell}_{21}\, \xi^{m'\ell'}_{43}\, G^{>}_{31}(t',t)\, G^{<}_{24}(t,t'), \tag{B13}$$

$$G^{>}_{m\ell,m'\ell'}(t,t') = i\sum_{\substack{S_1,S_2\\S_3,S_4}} \zeta_2\, \overset{*}{\xi}{}^{m\ell}_{34}\, \xi^{m'\ell'}_{12}\, G^{>}_{31}(t,t')\, G^{<}_{24}(t',t), \tag{B14}$$

$$D^{<}_{m,m'}(t,t') = i\sum_{\substack{S_1,S_2\\S_3,S_4}} \zeta_2\, \overset{*}{\chi}{}^{m}_{21}\, \chi^{m'}_{43}\, G^{>}_{31}(t',t)\, G^{<}_{24}(t,t'), \tag{B15}$$

$$D^{>}_{m,m'}(t,t') = i\sum_{\substack{S_1,S_2\\S_3,S_4}} \zeta_2\, \overset{*}{\chi}{}^{m}_{34}\, \chi^{m'}_{12}\, G^{>}_{31}(t,t')\, G^{<}_{24}(t',t), \tag{B16}$$

where the PP-NEGF Green function is defined in Eq. (8), and ζ_p is introduced below Eq. (10).

Finally, using the connection between the greater and retarded pseudoparticle Green functions[76]

$$2i\,\mathrm{Im}G^r_{12}(t,t') = G^{>}_{12}(t,t'), \tag{B17}$$

and substituting the Fourier transformed representations of the quasiparticles Green functions [Eqs. (B13)–(B16)] into the NEGF expressions for the fluxes [Eqs. (B1) and (B2)], leads to Eqs. (9) and (10).

APPENDIX C: DEPHASING WITHIN THE PP-NEGF FORMALISM

It is customary to introduce dephasing via coupling to a bath of harmonic oscillators.[77] In the paper we utilize the bath B_d coupled to the LUMO of molecule 1 in the molecular pump model [see Fig. 1(a)] as the source of dephasing in the system. The greater and lesser self-energies due to this coupling are given within the PP-NEGF formalism by the expression[64,75]

$$\Sigma^{B_d,<}_{12,34}(\omega) = -i\eta^{1x}_{12}\,\gamma^{B_d}\,\eta^{*1x}_{34} \times\{\theta(\omega)N_{B_d}(\omega)+\theta(-\omega)[1+N_{B_d}(-\omega)]\}, \quad \text{(C1)}$$

$$\Sigma^{B_d,>}_{12,34}(\omega) = -i\eta^{1x}_{12}\,\gamma^{B_d}\,\eta^{*1x}_{34} \times\{\theta(\omega)[1+N_{B_d}(\omega)]+\theta(-\omega)N_{B_d}(-\omega)\}, \quad \text{(C2)}$$

where $\theta(x)$ is the Heaviside step function, and γ^{B_d} and η^{1x}_{pg} are introduced below Eq. (15).

Finite frequencies of the oscillators in the bath induce energy flow in the system. In addition to dephasing, this may cause inelastic effects in both charge and energy fluxes. To avoid this scenario we assume that the bath oscillators have zero frequency and all in the ground state. From the physical point of view, this assumption is valid when the relevant energy scales in the system (for example, the HOMO-LUMO gap) are much bigger than the frequencies of vibrations in the environment. Taking the limit of $\omega_\alpha \to 0$ under the restriction $N_{B_d}(\omega) = 0$ leads to Eq. (15).

*ajw009@ucsd.edu
†uri@tx.technion.ac.il
‡migalperin@ucsd.edu

[1] C. Patoux, C. Coudret, J.-P. Launay, C. Joachim, and A. Gourdon, Inorg. Chem. **36**, 5037 (1997).
[2] M. Mayor, H. B. Weber, J. Reichert, M. Elbing, C. von Hänisch, D. Beckmann, and M. Fischer, Angew. Chem. Int. Ed. **47**, 5834 (2003).
[3] H. Vazquez, R. Skouta, S. Schneebeli, M. Kamenetska, R. Breslow, L. Venkataraman, and M. Hybertsen, Nat. Nanotech. **7**, 663 (2012).
[4] S. Ballmann, R. Härtle, P. B. Coto, M. Elbing, M. Mayor, M. R. Bryce, M. Thoss, and H. B. Weber, Phys. Rev. Lett. **109**, 056801 (2012).
[5] A. Assion, T. Baumert, M. Bergt, T. Brixner, B. Kiefer, V. Seyfried, M. Strehle, and G. Gerber, Science **282**, 919 (1998).
[6] M. Shapiro and P. Brumer, *Principles of the Quantum Control of Molecular Processes* (Wiley, New York, 2003).
[7] K. Hornberger, S. Gerlich, P. Haslinger, S. Nimmrichter, and M. Arndt, Rev. Mod. Phys. **84**, 157 (2012).
[8] M. Galperin and A. Nitzan, Phys. Chem. Chem. Phys. **14**, 9421 (2012).
[9] M. Grifoni and P. Hänggi, Phys. Rep. **304**, 229 (1998).
[10] S. Kohler, J. Lehmann, and P. Hänggi, Superlattices Microstruct. **34**, 419 (2003).
[11] S. Kohler, J. Lehmann, and P. Hänggi, Phys. Rep. **406**, 379 (2005).
[12] K. A. Pronin and A. D. Bandrauk, Phys. Rev. B **69**, 195308 (2004).
[13] G. Li, M. Schreiber, and U. Kleinekathöfer, New J. Phys. **10**, 085005 (2008).
[14] U. Peskin and M. Galperin, J. Chem. Phys. **136**, 044107 (2012).
[15] A. Ridolfo, O. Di Stefano, N. Fina, R. Saija, and S. Savasta, Phys. Rev. Lett. **105**, 263601 (2010).
[16] S. M. Morton and L. Jensen, J. Chem. Phys. **135**, 134103 (2011).
[17] A. Manjavacas, F. J. G. d. Abajo, and P. Nordlander, Nano Lett. **11**, 2318 (2011).
[18] A. Salomon, R. J. Gordon, Y. Prior, T. Seideman, and M. Sukharev, Phys. Rev. Lett. **109**, 073002 (2012).
[19] Y. Gao and D. Neuhauser, J. Chem. Phys. **137**, 074113 (2012).
[20] H. Lee, Y.-C. Cheng, and G. R. Fleming, Science **316**, 1462 (2007).
[21] G. S. Engel, T. R. Calhoun, E. L. Read, T.-K. Ahn, T. Mancal, Y.-C. Cheng, R. E. Blankenship, and G. R. Fleming, Nature (London) **446**, 782 (2007).
[22] G. Panitchayangkoon, D. Hayes, K. A. Fransted, J. R. Caram, E. Harel, J. Wen, R. E. Blankenship, and G. S. Engel, Proc. Natl. Acad. Sci. USA **107**, 12766 (2010).
[23] A. Ishizaki, T. R. Calhoun, G. S. Schlau-Cohen, and G. R. Fleming, Phys. Chem. Chem. Phys. **12**, 7319 (2010).
[24] R. Hildner, D. Brinks, and N. F. van Hulst, Nat. Phys. **7**, 172 (2011).
[25] R. Baer and D. Neuhauser, J. Am. Chem. Soc. **124**, 4200 (2002).
[26] R. Baer and D. Neuhauser, Chem. Phys. **281**, 353 (2002).
[27] D. M. Cardamone, C. A. Stafford, and S. Mazumdar, Nano Lett. **6**, 2422 (2006).
[28] C. A. Stafford, D. M. Cardamone, and S. Mazumdar, Nanotechnology **18**, 424014 (2007).
[29] D. Brisker, I. Cherkes, C. Gnodtke, D. Jarukanont, S. Klaiman, W. Koch, S. Weissman, R. Volkovich, M. C. Toroker, and U. Peskin, Mol. Phys. **106**, 281 (2008).
[30] Z. Qian, R. Li, X. Zhao, S. Hou, and S. Sanvito, Phys. Rev. B **78**, 113301 (2008).
[31] S.-H. Ke, W. Yang, and H. U. Baranger, Nano Lett. **8**, 3257 (2008).
[32] T. Hansen, G. C. Solomon, D. Q. Andrews, and M. A. Ratner, J. Chem. Phys. **131**, 194704 (2009).
[33] R. E. Sparks, V. M. García-Suárez, D. Z. Manrique, and C. J. Lambert, Phys. Rev. B **83**, 075437 (2011).
[34] O. Hod, R. Baer, and E. Rabani, Phys. Rev. Lett. **97**, 266803 (2006).
[35] R. Volkovich, M. C. Toroker, and U. Peskin, J. Chem. Phys. **129**, 034501 (2008).
[36] S. S. Skourtis, D. H. Waldeck, and D. N. Beratan, J. Phys. Chem. B **108**, 15511 (2004).
[37] R. Härtle, M. Butzin, O. Rubio-Pons, and M. Thoss, Phys. Rev. Lett. **107**, 046802 (2011).
[38] I. Sinayskiy, A. Marais, F. Petruccione, and A. Ekert, Phys. Rev. Lett. **108**, 020602 (2012).
[39] J. Repp, P. Liljeroth, and G. Meyer, Nat. Phys. **6**, 975 (2010).
[40] D. Xiao, S. S. Skourtis, I. V. Rubtsov, and D. N. Beratan, Nano Lett. **9**, 1818 (2009).
[41] M. Galperin and A. Nitzan, J. Phys. Chem. B **117**, 4449 (2013).

[42]A. Ishizaki and G. R. Fleming, Proc. Natl. Acad. Sci. USA **106**, 17255 (2009).
[43]A. Ishizaki and G. R. Fleming, J. Chem. Phys. **130**, 234111 (2009).
[44]C. Olbrich, T. L. C. Jansen, J. Liebers, M. Aghtar, J. Strümpfer, K. Schulten, J. Knoester, and U. Kleinekathöfer, J. Phys. Chem. B **115**, 8609 (2011).
[45]N. Renaud, M. A. Ratner, and V. Mujica, J. Chem. Phys. **135**, 075102 (2011).
[46]A. W. Chin, J. Prior, R. Rosenbach, F. Caycedo-Soler, S. F. Huelga, and M. B. Plenio, Nat. Phys. **9**, 113 (2013).
[47]B. N. J. Persson, Chem. Phys. Lett. **82**, 561 (1981).
[48]M. Oren, M. Galperin, and A. Nitzan, Phys. Rev. B **85**, 115435 (2012).
[49]M. Galperin, A. Nitzan, and M. A. Ratner, Phys. Rev. Lett. **96**, 166803 (2006).
[50]M. Galperin and A. Nitzan, J. Chem. Phys. **124**, 234709 (2006).
[51]B. D. Fainberg, M. Sukharev, T.-H. Park, and M. Galperin, Phys. Rev. B **83**, 205425 (2011).
[52]A. J. White, B. D. Fainberg, and M. Galperin, J. Phys. Chem. Lett. **3**, 2738 (2012).
[53]R. Härtle, U. Peskin, and M. Thoss, Phys. Status Solidi (b) **250**, 2365 (2013).
[54]G. Q. Li, B. D. Fainberg, A. Nitzan, S. Kohler, and P. Hänggi, Phys. Rev. B **81**, 165310 (2010).
[55]G. Li, M. S. Shishodia, B. D. Fainberg, B. Apter, M. Oren, A. Nitzan, and M. A. Ratner, Nano Lett. **12**, 2228 (2012).
[56]J. Fransson and M. Galperin, Phys. Rev. B **81**, 075311 (2010).
[57]J. Fransson and M. Galperin, Phys. Chem. Chem. Phys. **13**, 14350 (2011).
[58]D. Rai and M. Galperin, Phys. Rev. B **86**, 045420 (2012).
[59]D. Rai and M. Galperin, J. Phys. Chem. C **117**, 13730 (2013).
[60]S. Datta, *Electronic Transport in Mescoscopic Systems* (Cambridge University Press, Cambridge, 1995).
[61]P. Zhang, Q.-K. Xue, and X. C. Xie, Phys. Rev. Lett. **91**, 196602 (2003).
[62]B. Wang, J. Wang, and H. Guo, Phys. Rev. B **67**, 092408 (2003).
[63]J. Fransson and J.-X. Zhu, Phys. Rev. B **78**, 113307 (2008).
[64]A. J. White and M. Galperin, Phys. Chem. Chem. Phys. **14**, 13809 (2012).
[65]I. Kinoshita, A. Misu, and T. Munakata, J. Chem. Phys. **102**, 2970 (1995).
[66]D. Porath, A. Bezryadin, S. de Vries, and C. Dekker, Nature (London) **403**, 635 (2000).
[67]K. Schwab, E. A. Henriksen, J. M. Worlock, and M. L. Roukes, Nature (London) **404**, 974 (2000).
[68]M. Leijnse and M. R. Wegewijs, Phys. Rev. B **78**, 235424 (2008).
[69]M. Esposito and M. Galperin, Phys. Rev. B **79**, 205303 (2009).
[70]M. Esposito and M. Galperin, J. Phys. Chem. C **114**, 20362 (2010).
[71]M. G. Schultz and F. von Oppen, Phys. Rev. B **80**, 033302 (2009).
[72]H. Haug and A.-P. Jauho, *Quantum Kinetics in Transport and Optics of Semiconductors*, Vol. 123 of Springer Series in Solid-State Sciences, 2nd ed. (Springer, Berlin, 2008).
[73]M. Galperin, A. Nitzan, and M. A. Ratner, Phys. Rev. B **75**, 155312 (2007).
[74]G. D. Mahan, *Many-Particle Physics* (Plenum, New York, 1990).
[75]M. Galperin, M. A. Ratner, and A. Nitzan, J. Chem. Phys. **121**, 11965 (2004).
[76]N. S. Wingreen and Y. Meir, Phys. Rev. B **49**, 11040 (1994).
[77]M. P. Anantram and S. Datta, Phys. Rev. B **51**, 7632 (1995).